energies

MDPI

Article

Evaluating the Degree of Tectonic Fracture Development in the Fourth Member of the Leikoupo Formation in Pengzhou, Western Sichuan, China

Qiang Xie [1], Gao Li [1,*], Xu Yang [1] and Hongli Peng [2]

[1] State Key Laboratory of Oil and Gas Reservoir Geology and Exploration, Southwest Petroleum University, Chengdu 610500, China
[2] Petroleum Engineering Technology Research Institute, SINOPEC Southwest Oil & Gas Branch, Deyang 618000, China
* Correspondence: ligao@swpu.edu.cn; Tel.: +86-156-8063-5258

Abstract: The extent of fracture development is associated with the degree of enrichment of a natural gas reservoir and its productivity. Based on numerical simulation results of the paleotectonic stress field, a set of evaluation methods for determining the degree of development of reservoir tectonic fractures were established using rock rupture criteria. Taking the fourth member of the Leikoupo Formation in the Pengzhou area of western Sichuan as an example, a finite element (FE) method was employed to simulate the paleo-tectonic stress field during the period of fracture development, and the degree of tectonic fracture development was further evaluated using the above methods. The results indicated that effective fractures were created in the Himalayan period. In this time, mainly NE–NEE and nearly E–W strike tectonic fractures were developed in the target layer. The fractures were mainly low-angle and oblique fractures, while the high-angle fractures were less developed. According to the integrative fracture index (*F*), five typical fracture development areas were determined: the fault zone, and the northern, eastern, southeastern, and central regions of the study area. The reliability of the fracture prediction results was verified using fracture distribution statistics and gas production test results.

Keywords: tectonic fracture; fracture development degree; evaluation method; Leikoupo Formation; Himalayan period

Citation: Xie, Q.; Li, G.; Yang, X.; Peng, H. Evaluating the Degree of Tectonic Fracture Development in the Fourth Member of the Leikoupo Formation in Pengzhou, Western Sichuan, China. *Energies* **2023**, *16*, 1797. https://doi.org/10.3390/en16041797

Academic Editors: Hu Li, Ahmed E. Radwan and Shuai Yin

Received: 6 January 2023
Revised: 2 February 2023
Accepted: 10 February 2023
Published: 11 February 2023

1. Introduction

With improvements in the level oil and gas exploration, fractured reservoirs have acquired a significant position in the distribution of oil and gas fields around the world [1,2]. In fractured reservoirs, fractures represent the main channels for fluid seepage and oil and gas migration, and they control the formation and distribution of oil and gas reservoirs [3–5]. The fourth member of the Leikoupo (T_2l^4) Formation in the Pengzhou area of western Sichuan is a typical fractured reservoir. Several natural gas accumulations have been discovered within this reservoir, making the area another major gas field after Puguang and Yuanba [6–9]. However, fractures complicate the geological conditions of the reservoir and create many problems for the exploration and development of the region [3,10,11]. Therefore, the study of fractures is of great significance for the rational development of natural gas in the Pengzhou area.

Fracture research has a history of more than one hundred years and has resulted in a number of distinctive research methods, including the geological method of outcrop, core, and cast thin section observation [12–14]; the geophysical method of seismic data and logging data analysis [15–18]; and the numerical simulation method of tectonic stress fields [19–21], etc. However, geological and geophysical methods require a large amount of basic geological data. The numerical simulation method of tectonic stress fields is suitable for areas with limited data.

In recent years, tectonic fractures have become a key object of research. Tectonic stress controls the development and distribution of tectonic fractures [20,22]. Therefore, the analysis of changes in regional stress is a popular approach for characterizing the distribution of fractures in an area. In previous studies, the relationships between the curvature, folds, and fracture characteristics have been studied using the rock rupture criterion and the main structure curvature method [23–25]. These studies have provided a foundation for predicting the development and distribution of tectonic fractures in these reservoirs. Meanwhile, in other studies, numerical simulation methods were employed to calculate regional tectonic stress fields, and the development of tectonic fractures in reservoirs was predicted based on the Griffith rupture and the Mohr–Coulomb criteria [3,26–29]. In addition, based on the numerical simulation results of the stress field, some studies predicted fracture initiation and propagation phenomena using the principle of rock fracture mechanics [30–32], and the research results explained the mechanism of fracture development to a certain extent, which has a guiding role in the fracturing and reconstruction of gas reservoirs. However, these studies only predicted the degree of development of tectonic fractures and did not further predict the distribution characteristics of fracture occurrence. Fracture occurrence plays a decisive role in quantifying the anisotropy of fractured reservoirs [33]. Therefore, it is very important to predict fracture occurrence and study the influence of the dip angle on the degree of fracture development, to accurately understand regional fracture distribution characteristics.

Owing to intense tectonic activity, the reservoirs in the Pengzhou area of western Sichuan involve fractures with multiple development stages and characteristics [9,34]. However, the distribution of fractures in these reservoirs has not been systematically interpreted, which restricts the effective development of these natural gas pools. Therefore, in this study, a finite element method was used to simulate the tectonic stress field during the fracture development period, and then a fracture occurrence calculation model and fracture prediction model were established on the basis of the rock rupture criteria. Finally, a set of evaluation methods for the degree development of reservoir tectonic fractures were formulated, and an evaluation was carried out of the degree of development of the reservoir tectonic fracture in the T_2l^4 Formation in the Pengzhou area, western Sichuan. The present study can provide a geological foundation for the exploration and development of reservoirs in the Pengzhou area.

2. Geological Setting

The Pengzhou area is the piedmont of Longmenshan in the Western Sichuan Depression. The Longmenshan Piedmont Tectonic Belt (LPTB) involves the Shiyangchang and the Jinma-Yazihe secondary structures (Figure 1). The Jinma-Yazihe structure is a NE-trending faulted anticline in the N, while the Shiyangchang structure is a NE-trending anticline with a short axis in the S. Pengxian and Guankou are two major reverse faults in the structural belt of the Western Sichuan Depression that sandwich the LPTB (Figure 1). The NE-striking Guankou Fault is situated in the northwest of the LPTB, while the NE-striking Pengxian Fault in the SE involves a plane inclined to the NW. In addition, minor interlayer faults are present within the main portion of the LPTB. These faults constitute a transport network through which oil and gas migration in the area primarily occurs. A platform margin evaporation/lagoon tidal flat carbonate depositional system has formed in the study area. The reservoirs in this area are mainly located in the intertidal zone, and the lithology of the reservoirs is mainly carbonate and dolomite mixed with gypsum [9].

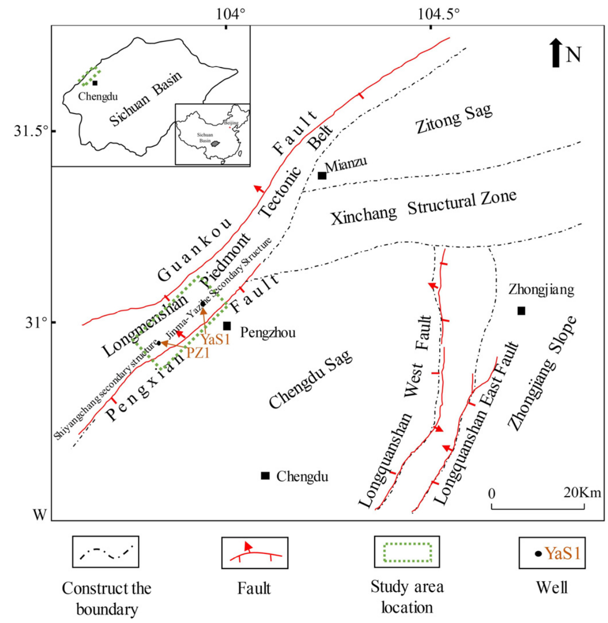

Figure 1. Structural unit division and location of the study area in the western Sichuan basin.

According to tectonic evolution studies of the area, the main structure of the LPTB emerged in the Late Indosinian period [34]. Entering the Yanshanian period, the structure continued to develop and terminated in the Himalayan period. This indicates that the Pengzhou area in western Sichuan has experienced several tectonic movements, and the tectonic fractures of the T_2l^4 Formation may exist in multiple stages. Previous studies have shown that the T_2l^4 reservoirs developed four stages of tectonic fractures [9,34]. The fracture development stages include the following periods (Figure 2): (1) the second phase of the Late Indosinian, (2) the third phase of the Late Indosinian to Early-Middle Yanshanian, (3) the Middle to Late Yanshanian, and (4) the Himalayan. As illustrated in Figure 2, the tectonic fractures formed in the first three stages were mostly filled during diagenesis. After entering the Himalayan period, the diagenesis was less intense, and the newly formed tectonic fractures were unfilled. Furthermore, in the Himalayan period, the crude oil cracked and became natural gas, under the conditions of deep burial and high temperatures [35]. The unfilled tectonic fractures formed at this time became the main storage space and transportation channels for oil and gas. Therefore, the tectonic fractures formed during the Himalayan period were the focus of the present study.

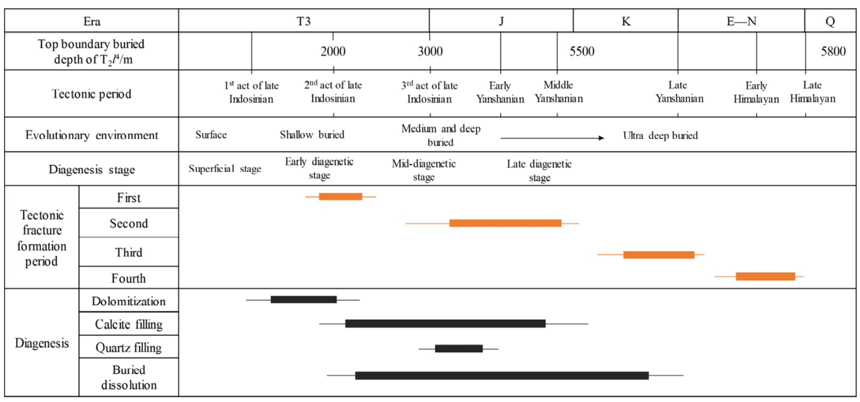

Figure 2. Sequence diagram of the tectonic fracture formation period and dissolution in the T_2l^4 reservoir.

3. Theory and Methods

3.1. Evaluation Process of Tectonic Fracture Development

Numerical simulation of tectonic stress fields using finite element methods can successfully obtain the distribution characteristics of the tectonic stress field during the fracture formation period. On this basis, the degree of development of regional tectonic fractures can be evaluated, in combination with the rock rupture criterion. Figure 3 presents the specific process for evaluating the degree of development of reservoir tectonic fractures. First, a real 3D structural model was built by combining the regional seismic interpretation results with the analysis of structural characteristics and tectonic evolution history, and the fault model was further embedded. Then, based on acoustic emissions, rock mechanics test results, and logging data, a three-dimensional heterogeneous mechanical model was established, and numerical simulation of the paleotectonic stress field was carried out. According to the numerical simulation results and rock rupture criteria, a fracture occurrence calculation model and fracture prediction model were established, to evaluate the degree development of tectonic fractures in the reservoir.

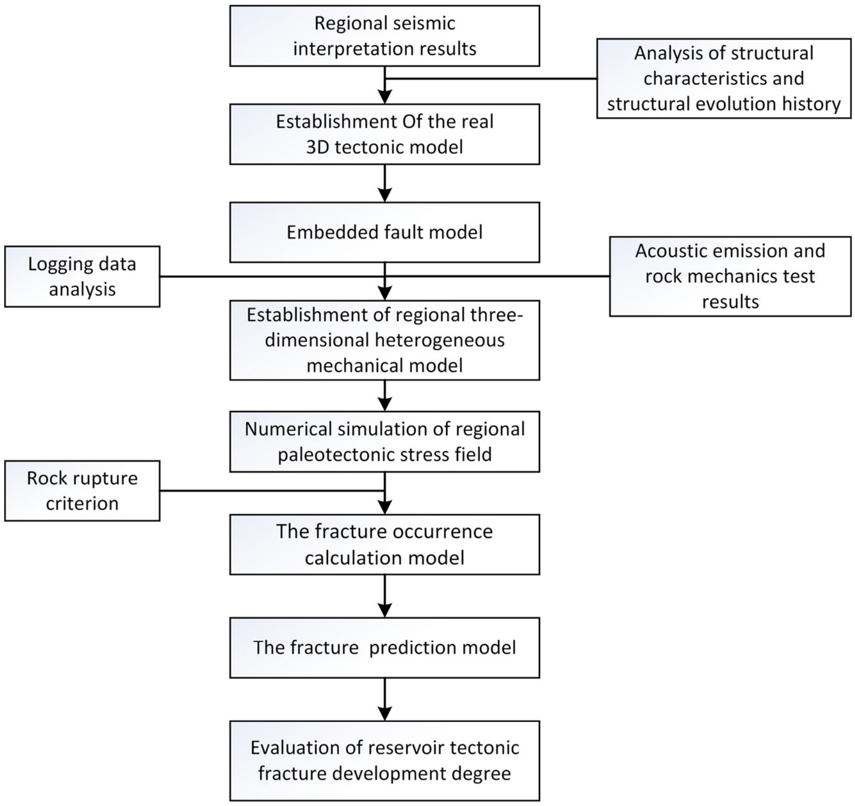

Figure 3. Flow chart for evaluation of the reservoir tectonic fracture development.

3.2. Fracture Occurrence Calculation Model

When the rock is subjected to the action of stress, it will rupture, and the form of rupture is generally developed into tensile fractures or shear fractures. Therefore, fracture occurrence can be calculated using the numerical simulation results of the tectonic stress field combined with the rock rupture criterion. The Griffith and Mohr–Coulomb criteria are widely used to investigate rock rupture under compressive and tensile stress conditions, respectively. The Griffith criterion is expressed in the following:

$$\begin{cases} (\sigma_1-\sigma_3)^2+(\sigma_2-\sigma_3)^2+(\sigma_3-\sigma_1)^2=24\sigma_T(\sigma_1+\sigma_2+\sigma_3) \\ \cos 2\theta = \frac{\sigma_1-\sigma_3}{2(\sigma_1+\sigma_3)} \end{cases}, \text{ if } \sigma_1+3\sigma_3>0 \text{ and } \sigma_3<0 \quad (1)$$

$$\begin{cases} \sigma_3 = -\sigma_T \\ \theta = 0 \end{cases}, \text{ if } \sigma_1 + 3\sigma_3 \leq 0 \text{ and } \sigma_3 < 0 \tag{2}$$

where σ_1, σ_2, and σ_3 are the maximum, intermediate, and minimum principal stresses, respectively, Pa; σ_T is the tensile stress on the fracture surface, Pa; and θ is the rupture angle, °.

When compressive stress exists, the Mohr–Coulomb formula is expressed as follows:

$$[\tau] = C + \sigma_n \tan\varphi \tag{3}$$

$$\sigma_n = \frac{\sigma_1 + \sigma_3}{2} + \frac{\sigma_1 - \sigma_3}{2}\cos 2\theta \tag{4}$$

$$\tau_n = \frac{\sigma_1 - \sigma_3}{2}\sin 2\theta \tag{5}$$

$$\theta = \frac{\pi}{4} - \frac{\varphi}{2} \tag{6}$$

where $[\tau]$ is the shear strength, Pa; C is the cohesive strength, Pa; φ is the internal friction angle, °; σ_n is the normal stress on the shear plane, Pa; and τ_n is the shear stress, Pa.

Fracture occurrence can be calculated according to the fracture normal vector. It is assumed that $\mathbf{t}'$ is the normal vector of the fracture in the principal stress coordinate system (x', y', z'), where the principal stresses σ_1, σ_2, and σ_3 are aligned with x', y', and z', respectively. The normal vector $\mathbf{t}'$ is expressed in the global coordinate system (x, y, z) as follows [36]:

$$\mathbf{t} = \begin{bmatrix} t_x & t_y & t_z \end{bmatrix}^T \tag{7}$$

$$t_x = u_1 t_{x'} + u_2 t_{y'} + u_3 t_{z'} \tag{8}$$

$$t_y = v_1 t_{x'} + v_2 t_{y'} + v_3 t_{z'} \tag{9}$$

$$t_z = w_1 t_{x'} + w_2 t_{y'} + w_3 t_{z'} \tag{10}$$

$$t_{x'} = \sin\theta \quad t_{y'} = 0 \quad t_{z'} = \cos\theta(\text{or } -\cos\theta) \tag{11}$$

where u_i, v_i, and w_i (i = 1, 2, 3) are the direction cosines of principal stresses in the global coordinate system.

Then, the fracture occurrence can be obtained:

$$\eta = \arccos|t_z| \tag{12}$$

$$\gamma = \arctan\left(\frac{t_x}{t_y}\right) \tag{13}$$

$$\xi = \begin{cases} \gamma - 90^\circ, & \gamma > 90^\circ \\ \gamma + 90^\circ, & \gamma < 90^\circ \end{cases} \tag{14}$$

where η is the fracture dip angle, °; γ is the fracture dipping direction, °; and ξ is the fracture strike direction, °.

3.3. Fracture Prediction Model

According to the Griffith criterion, when the tensile stress of the rock is greater than or equal to its tensile strength, the rock will rupture, forming tensile fractures. In order to characterize the degree development of tensile fractures in the target layer, the tensile fracture index (T) was utilized, and its mathematical expression is as follows:

$$T = \left|\frac{\sigma_T}{\sigma_t}\right| \tag{15}$$

where σ_t is the tensile strength of the rock, Pa. The extent of tensile fracture development is proportional to T.

Based on the Mohr–Coulomb criterion, when the shear stress on a rock is greater than or equal to its shear strength, shear failure occurs and shear fractures are formed. Similarly, the shear fracture index (S) was used to characterize the extent of development of shear fractures in the target layer, and its mathematical expression is as follows:

$$S = \left| \frac{\tau_n}{[\tau]} \right| \tag{16}$$

The extent of development of shear fractures is also proportional to S.

Tensile and shear fractures can be developed in the stratum; thereby, the extent of development of fractures should be determined by both systems of fractures. Consequently, the integrative fracture index (F) was incorporated into the evaluation of the extent of development of tectonic fractures, and its mathematical expression is as follows:

$$F = m \times T + n \times S \tag{17}$$

where m and n are the scale of tensile and shear fractures, respectively. The extent of development of the fracture system of the target layer is directly relevant to F.

The fracture degree of development also depends upon the fracture dip angle. F in Equation (17) refers to the degree of fracture development in the fracture's normal direction. The degree of fracture development in the vertical and horizontal directions can be calculated as follows:

$$\begin{cases} F_z = F\cos\eta \\ F_h = F\sin\eta\cos(|\alpha - \gamma|) \end{cases} \tag{18}$$

where F_z is the fracture index in the vertical direction; F_h is the fracture index in the horizontal direction; and α is the azimuth, °. It is obvious from Equation (18) that the direction of the maximum horizontal fracture index is parallel to the fracture dipping direction (i.e., $\alpha = \gamma$).

4. Paleotectonic Stress Field Simulation

The Himalayan movement represents the period of most intense tectonic activity in the western Sichuan depression [34]. Therefore, tectonic fractures in the T_2l^4 Formation are closely linked to these activities. Reconstructing the tectonic stress fields in this formation during the Himalayan period is crucial for understanding the development of the associated fractures. In the present study, the finite element method was employed to simulate the tectonic stress field in the Pengzhou area during this period. The simulation steps, which were described in Guo et al. [26], are summarized as follows: (1) establishment of a structural model of the study area, (2) determination of the mechanical parameters of rocks in the area, (3) assignment of boundary conditions, and (4) finite element calculation.

4.1. Establishment of Structural Model

A reasonable and accurate structural model is the key to the numerical simulation of the tectonic stress field. Based on the seismic interpretation results, the point cloud data of the top surface of the T_2l^4 Formation in the Pengzhou area of the Sichuan Basin was obtained. Then, the point cloud data were imported into the reverse engineering software 3DMove, to establish a structural surface model. Next, the structural surface model was imported into the finite element software COMSOL, to establish a structural geometry model, and the interpreted faults were further embedded into the geometric model. Finally, a 3D structural model of the target layer in the study area was established; the modeling process is shown in Figure 4. The study area was approximately 32.4 km from NE to SW, and 13.6 km from NW to SE. In total, 23 major faults were considered in the established model. To decrease the influence of border effects on the calculations, the study area was isolated from the overburden and basement during the simulation (Figure 5).

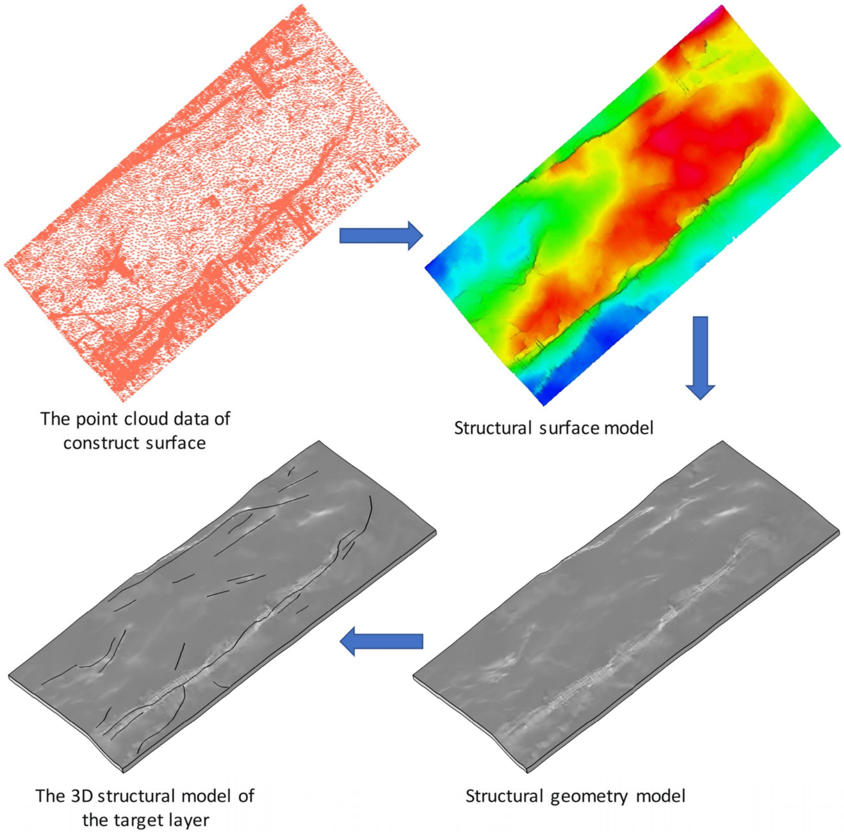

Figure 4. Construction process of the 3D construction model of the target layer.

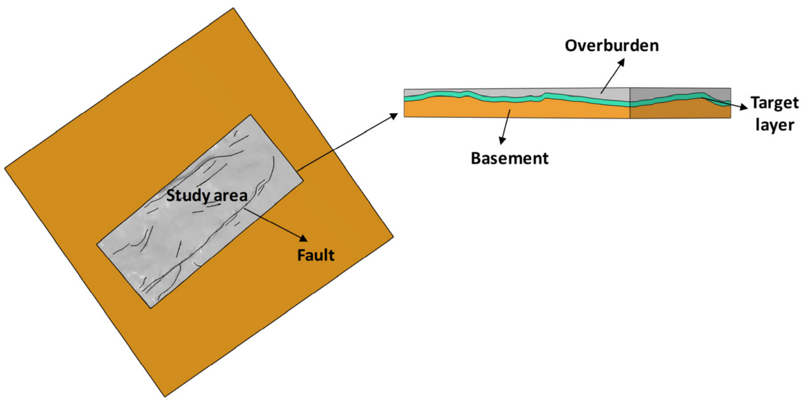

Figure 5. Three-dimensional structure model of the target layer in the study area.

4.2. Determination of Mechanical Parameters

After the structural model was successfully obtained, it was transformed into a mechanical model that could be numerically calculated. The Young's modulus, Poisson's ratio, and bulk density of the rock were important parameters for the numerical simulation of the tectonic stress field. Velocities of P- and S-waves were obtained on the basis of logging data, while the dynamic Young's modulus (E_d) was calculated using the following equation [37]:

$$E_d = \frac{DEN}{V_s^2} \frac{3V_s^2 - 4V_p^2}{V_s^2 - V_p^2} \tag{19}$$

where DEN represents the bulk density of the rocks, g/cm^3; V_s represents the shear wave slowness, μs/ft; and V_p represents the compressional wave slowness, μs/ft.

However, in the FE calculation of the tectonic stress fields, adopting static parameters that reflect the mechanical properties of rocks in the formation is necessary. Based on the data obtained from the rock mechanics tests, a relationship was established between the dynamic and static Young's modulus (Figure 6). The calculated static elastic modulus obtained from the logging data, and the Poisson's ratio and rock density determined through the rock mechanic tests, served as parameters for the target layer. Moreover, the faults developed in the study area could have directly affected the results of the numerical simulation, so the rock mechanics parameters of the faults needed to be defined. Generally speaking, the fault zone is defined as a transition zone, and its mechanical parameters are related to those of the surrounding rock. The elastic modulus of the fault zone is generally 60% of the surrounding medium, and the Poisson's ratio of a fault zone is larger than that of a corresponding normal stratum [38,39]. According to the practice of many oilfields, the tensile and shear strength of a fault zone are also 60% of the corresponding mechanical parameters of the rock [19,39]. Consequently, the rock mechanics parameters for the numerical simulation of the tectonic stress field were determined, as shown in Table 1.

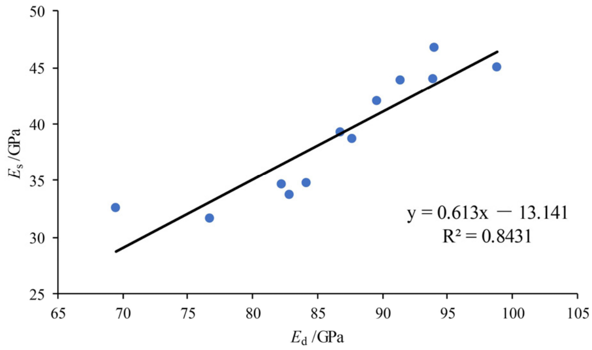

Figure 6. Plot showing the relationship between the dynamic (E_d) and static (E_s) Young's modulus.

Table 1. Data for rock mechanical parameters used in the numerical simulation.

Strata	E (GPa)	μ	ρ/(g/cm^3)	C (MPa)	ϕ (°)	σ_t (MPa)
T_2l^4	—	0.24	2.8	41.42	33.6	4.75
Overburden/surrounding rock	35.0	0.25	2.7	30.18	26.8	4.23
Basement	55.0	0.22	3.1	50.32	40.8	7.65
Faults	26.9	0.29	2.5	27.10	21.8	2.54

E—Young's modulus; μ—Poisson's ratio; ρ—density of rock; C—cohesion of rock; ϕ—internal friction angle; σ_t—tensile strength of rock.

4.3. Determining the Boundary Conditions

Boundary forces applied on the model boundaries included the horizontal tectonic stress, overburden pressure, and self-gravity [40]. The gravity of the model was expressed as the product of rock density and gravitational acceleration. Meanwhile, to decrease the influence of border effects and easily impose constraints, the loading boundary was set outside the study area, so that the horizontal tectonic stress was vertically applied to the boundary [29].

The depth of the model was associated with the z-axis, which involved a positive load, while the x-axis was directed to the E, and the y-axis was directed to the N. The analysis of the tectonic evolution, fracture formation times, and occurrence of conjugate shear fractures in the study area suggested that the direction of the maximum principal stress during the Himalayan period was nearly NESW. Based on the acoustic emission experiment, the maximum principal stress during the Himalayan period varied between 119.8 and 140.6 MPa, with an average of 131.2 MPa, and the minimum principal stress varied between 95.5 and 104.1 MPa, with an average of 101.3 MPa. Therefore, the boundary conditions for the simulation of the tectonic stress field during the Himalayan period (Figure 7) were as follows: a pressure of 131.2 MPa was utilized in the near NE–SW direction (NE235°), while a pressure of 101.3 MPa was utilized in the nearly NW–SE direction (NE145°). Meanwhile, constraints on the x-, y-, and z-directions were imposed on the nearly NE, nearly NW, and bottom boundaries of the model, respectively.

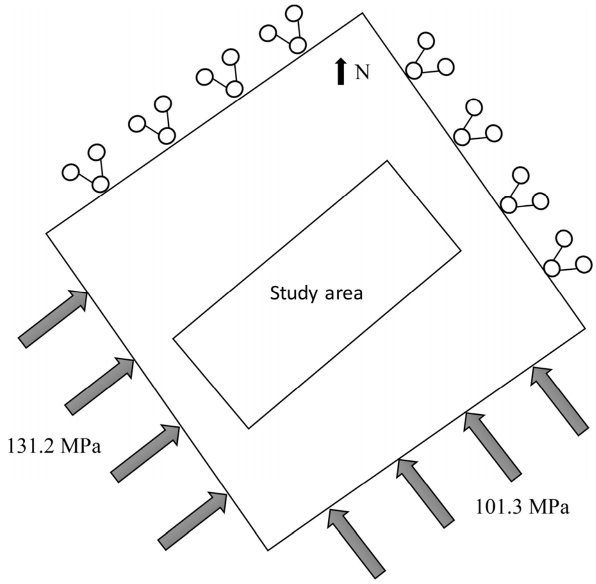

Figure 7. Illustration of the mechanical model for the Pengzhou area during the Himalayan Period.

4.4. Meshing and Numerical Simulation

In the numerical simulation of the paleotectonic stress field, Solid45 element was used to grid the model, in which the grid at the fault zone was densified, while the overlying strata and surrounding rock were sparsely meshed, to improve the calculation efficiency. The model was divided into 185,405 grid cells and 32,192 grid nodes, as shown in Figure 8.

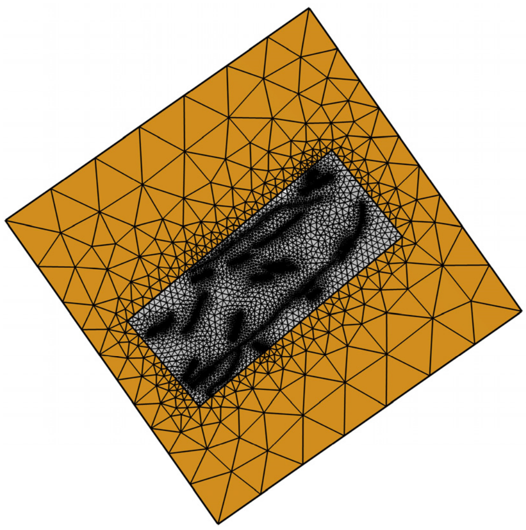

Figure 8. Finite element meshing diagram.

5. Results and Discussion

5.1. Paleotectonic Stress Field in the Himalayan

The Himalayan tectonic stress field in the study area was numerically simulated using COMSOL, and the results are shown in Figure 9. The results indicate that the maximum principal stress distribution range was 100–170 MPa, the intermediate principal stress distribution range was 95–140 MPa, and the minimum principal stress varied between 60 and 110 MPa. The stress distribution was highly dependent on the geographical location. The burial depth in the south and southwest of the study area is much deeper, leading to higher vertical stresses. The corresponding high stress is mainly concentrated in these areas. The central part of the study area belongs to the core of the anticline, where the stress values are relatively low. The stress distribution also depends upon the mechanical properties. It was found that the stresses in the fault zone were much lower than in other areas, due to the smaller elastic modulus in the fault zones, while the stress value in the vicinity of the fault zone was high. This phenomenon can be explained by the relative weakness of the interior portion of the fault zone, which is characterized by stress release and rock fracture [41]. Rocks around the fault zone show signs of deformation and are in a state of stress concentration [42]. The target layer in the study area is under the compressive stress environment, resulting in a high level of development of shear fractures. The above results indicate that the distribution characteristics of the regional stress field are controlled by multiple factors, such as the burial depth, the structural position, and the mechanical properties, etc.

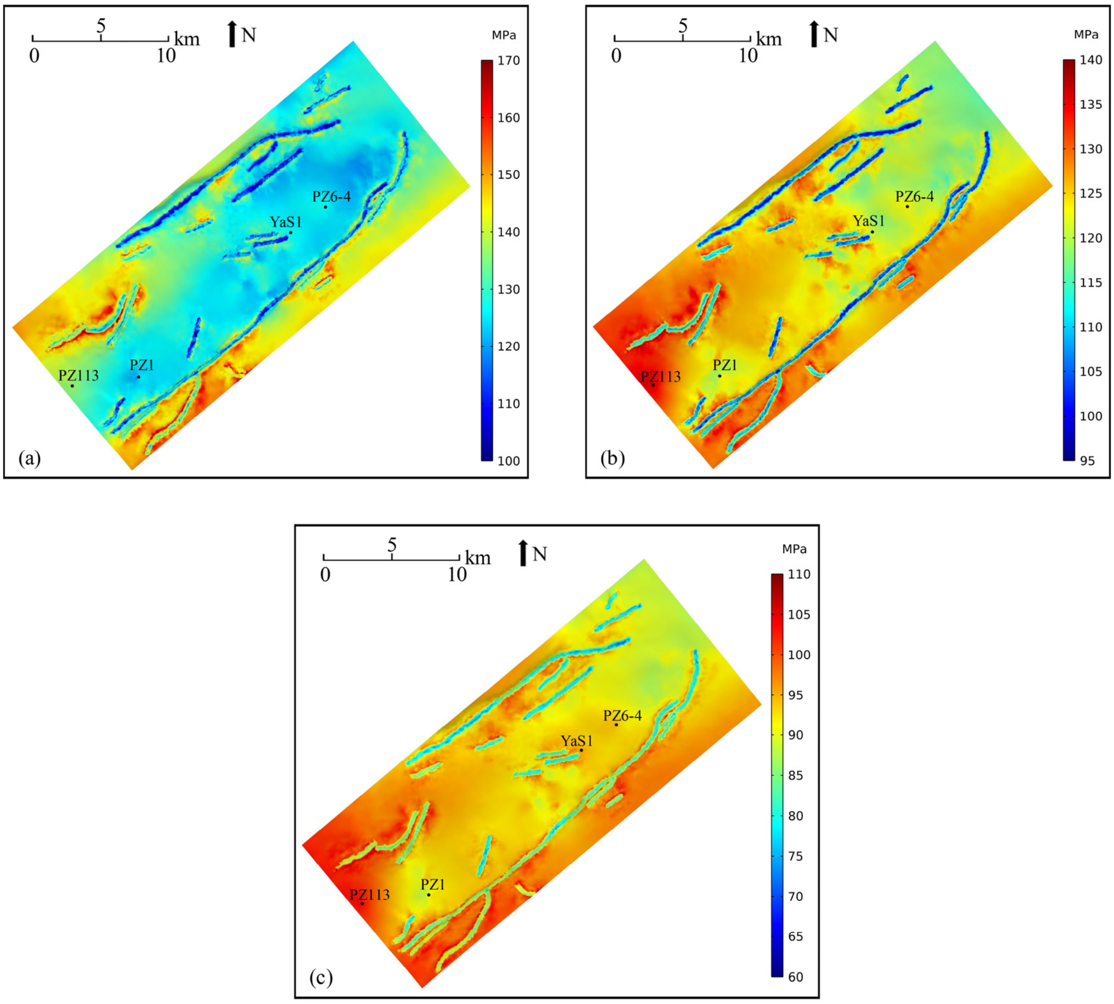

Figure 9. Plots showing the paleotectonic stress fields for the T_2l^4 Formation in the Pengzhou area during the Himalayan period. (**a**) Maximum principal stress, (**b**) intermediate principal stress, and (**c**) minimum principal stress.

5.2. Evaluation of the Degree of Development of Tectonic Fractures

According to the paleotectonic stress field simulation, the degree of development of tectonic fractures in the target strata during the Himalayan epoch was evaluated. Equations (1)–(18) were coded in MATLAB and automatically calculated in COMSOL. Figure 10 presents the distribution of the strike and dip angles of the tectonic fractures during the Himalayan period. Two main groups of tectonic fractures were developed in the study area, with corresponding strikes of NE–NEE and nearly E–W, respectively. The fractures in the nearly E–W strike were mostly concentrated in the central part of the study area, while the fractures in the NE–NEE strike were mainly developed in other areas. Moreover, two groups of fault-related fractures were developed around the fault zones: one group (NE-NEE) had the same strike as the fault, while the other group (nearly E–W) had a conjugate shear relationship with the fault. It can be seen from Figure 10b that low-angle fractures (<30°) and oblique fractures (30°–60°) were predominantly developed in the study area. The fractures in the NE–NEE strike were mainly low-angle fractures, while the fractures in the nearly E–W strike were generally oblique.

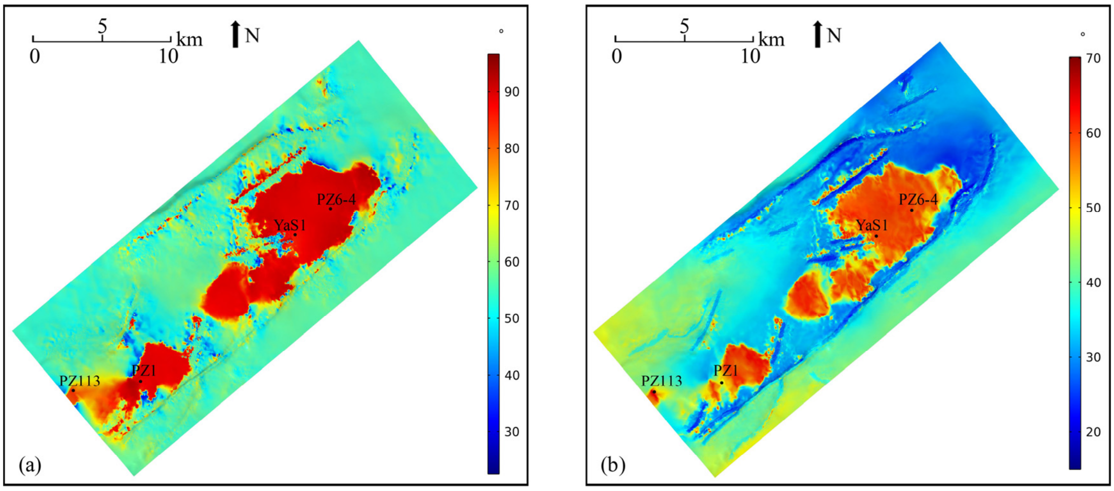

Figure 10. Distribution of the tectonic fractures in the T_2l^4 Formation during the Himalayan period. (**a**) Prediction of the tectonic fracture strike, and (**b**) prediction of the dip angle of the tectonic fracture.

Figure 11 shows the prediction results of the degree development of tectonic fractures in the target strata of the study area. The *F* value of the fault zone was greater than 1.6, indicating that the tectonic fractures in the fault zone were highly developed. In addition, the *F* values of the northern, eastern, and southeastern regions of the study area were also large, at approximately 1.3, which shows a relatively high degree of tectonic fracture development. Compared with the above areas, the *F* value of the central region of the study area was relatively smaller, approximately 1.1, indicating a relatively low degree of fracture development. The *F* value in the southwest of the study area was less than 1, which indicates that the tectonic fractures are essentially undeveloped in this area. The results show that the degree development of tectonic fractures in the study area was controlled by both structures and faults.

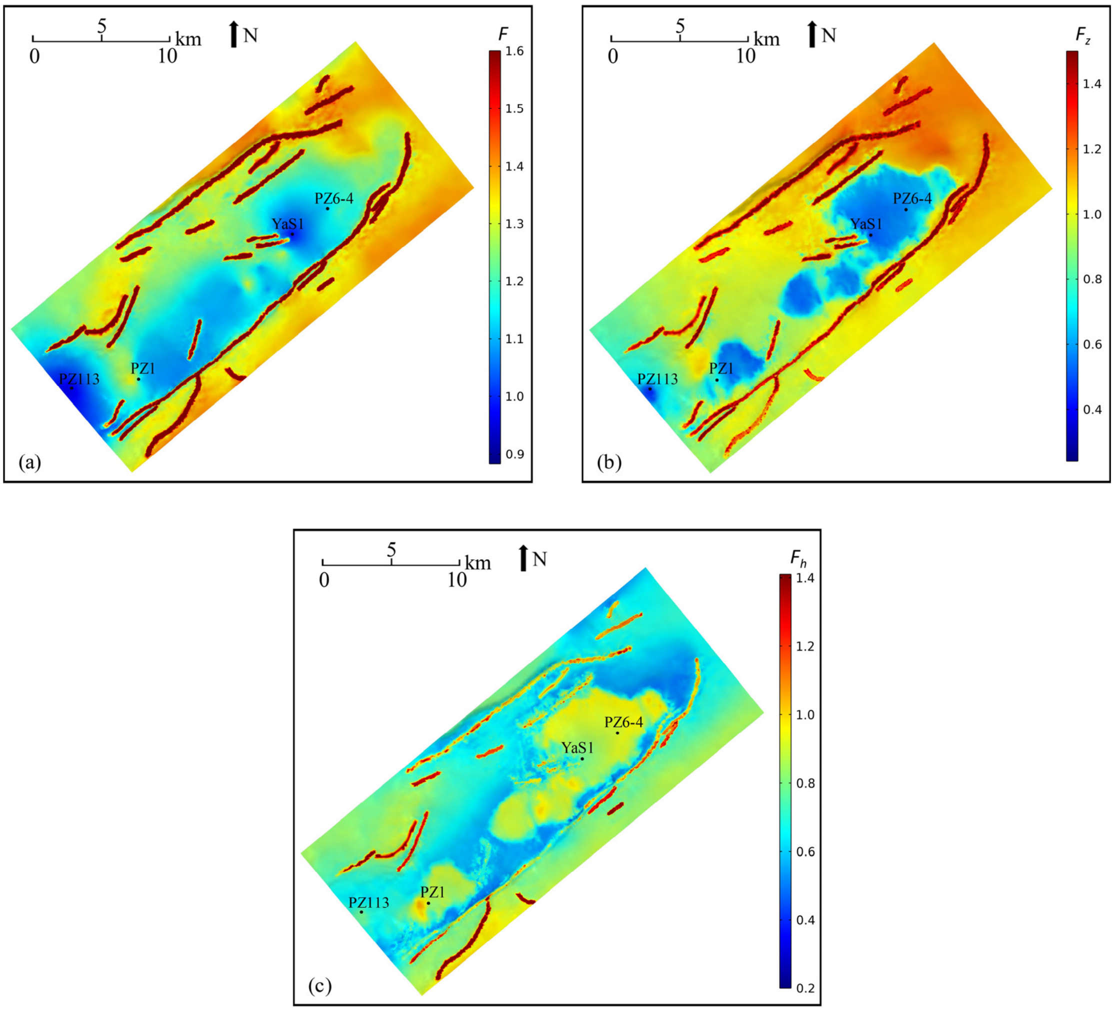

Figure 11. Plots exhibiting the predicted distribution of the degree of tectonic fracture development in the T_2l^4 Formation during the Himalayan period. (**a**) The degree of fracture development in the fracture normal direction, (**b**) the degree of fracture development in the vertical direction, and (**c**) the degree of fracture development in the maximum horizontal direction.

In the anticlinal region, the value of F_h was greater than that of F_z, indicating that the degree of fracture development in the maximum horizontal direction was higher than that in the vertical direction. The degree of anisotropic fracture development depends on the geographical location and the fracture dip angle. Based on the prediction results of fracture occurrence, it is believed that oblique fractures and high-angle fractures are more likely to develop in the core area of the anticline, resulting in a lower degree of development of vertical fractures and a higher degree of development of horizontal fractures. This means that drilling horizontal wells in these areas is more likely to cause fractures. In other areas beyond the fault and anticline core, the value of F_z is larger than that of F_h, which indicates that the vertical fracture development is higher than the maximum horizontal fracture development, suggesting that mainly low-angle fractures have developed in these areas.

5.3. Validation of Prediction Results

According to the image-logging of the target layer in the study area (Figure 12a), the distribution characteristics of tectonic fractures in the T_2l^4 Formation were statistically analyzed. The statistical results of the fracture dip angle and strike are shown in Figure 12. The low-angle fractures (<30°) were highly developed in the reservoirs, followed by oblique fractures (30°–60°), and high-angle fractures (>60°) accounted for the lowest proportion of the entire fracture system (Figure 12b). The fracture strike exhibited mainly NE–NEE and subordinate nearly E–W directions (Figure 12c). The prediction results were in good agreement with the statistical results of fractures, which indicates that the prediction results were reasonable.

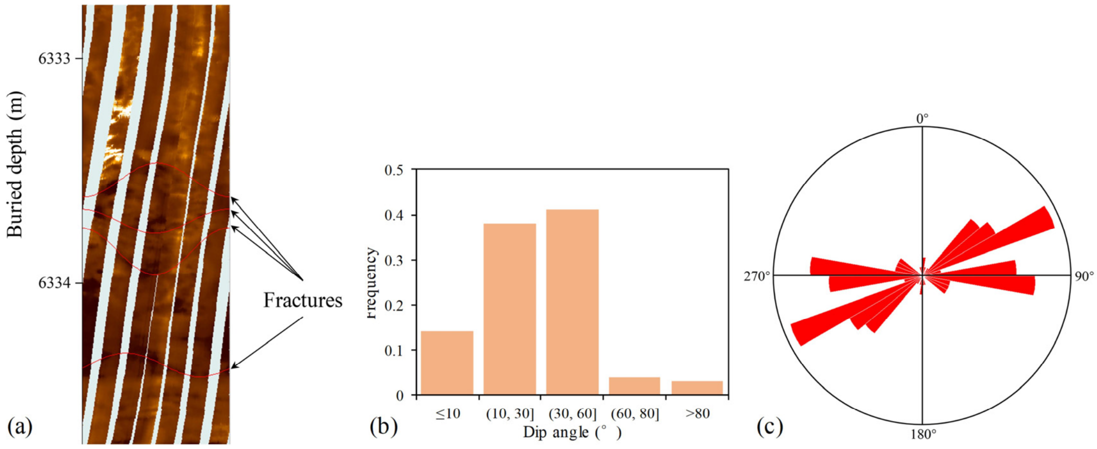

Figure 12. (**a**) Image-logging of well PZ1, (**b**) statistical results of fracture dip angle, and (**c**) rose diagram of fracture strike in the T_2l^4 Formation.

The open flow rates obtained from the gas production test of four wells in the study area were compared, as shown in Figure 13a. It should be noted that well PZ113 has the deepest burial depth, and the acid fracturing of this well failed due to the high fracturing pressure. In addition, well PZ1 has the largest open flow rate, exceeding 3 million m^3/d, followed by well PZ6-4, while well YaS1 has the smallest open flow rate. Meanwhile, it can be seen from Figure 13b that the F value of the PZ1, YaS1, and PZ6-4 wells was greater than 1, in which the F value of PZ1 was the largest, followed by that of PZ6-4, with that of YaS1 being the smallest, indicating that the degree of fracture development of the above three wells decreased successively. The open flow rates of the three wells had the same variation rule with a corresponding degree of fracture development. The above analysis further verified the accuracy of the fracture prediction results.

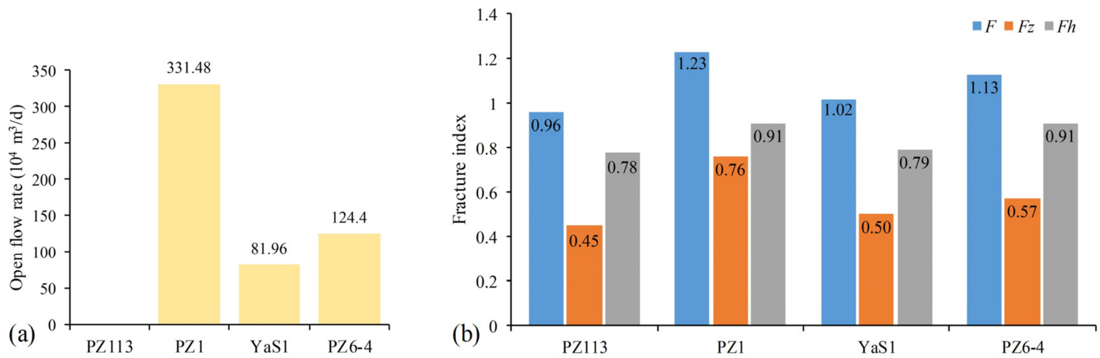

Figure 13. (**a**) Tested open flow rate of the four wells, and (**b**) fracture index of four wells in the study area.

Based on the above analysis, the degree of fracture development directly affects gas production. The anticline core in the study area mainly develops oblique fractures and high-angle fractures, and the F_h values in this area are high. For example, the wells PZ1, YaS1, and PZ6-4 located in this area have large F_h values, showing a relatively high degree of fracture development in the maximum horizontal direction. Considering that the core area of the anticline included in the PZ6-4 platform is the largest, it is suggested that future horizontal wells should be formed in the PZ6-4 platform. In this way, it would be easier to encounter fractures during drilling and obtain a higher production.

6. Conclusions

According to the numerical simulation results of the paleotectonic stress field, a fracture occurrence calculation model and fracture prediction model were established using rock rupture criteria, and finally a set of evaluation methods for the degree of development of reservoir tectonic fractures were formed. Taking the T_2l^4 Formation in the Pengzhou area of western Sichuan as an example, the tectonic stress field during the period of fracture development was simulated using FE. On this basis, the degree of tectonic fracture development was evaluated using the above methods. The following conclusions were drawn:

(1) The formation of tectonic fractures in the T_2l^4 Formation involved four stages. The ineffective fractures were mostly developed during the first three stages, whereas effective fractures that formed the main storage space and transportation channels for oil and gas were created in the last stage, which corresponds to the Himalayan period.
(2) The maximum, intermediate, and minimum principal stresses of the target layer during the Himalayan movement period were 100–170 MPa, 95–140 MPa, and 60–110 MPa, respectively. The distribution of paleotectonic stress was mainly controlled by the burial depth of the stratum, the structural position, and faults. The stress in the fault zone was much lower than in other regions, while the stress near the fault zone tended to increase due to differences in mechanical properties.
(3) Two main groups of tectonic fractures were developed in the Himalayan period, with the corresponding strikes of NE–NEE and nearly E–W, respectively. The fractures were mainly low-angle and oblique fractures, while high-angle fractures were less developed. The nearly E–W strike fractures, which were chiefly concentrated in the central part of the study area, were usually oblique and high-angle fractures. The NE–NEE strike fractures, which were mostly developed in other areas, were mainly low-angle fractures.
(4) The distribution of tectonic fractures in the study area was controlled by both structures and faults. The degree of fracture development was the highest in the fault zone, followed by the northern, eastern, and southeastern regions of the study area, while the degree of fracture development was relatively low in the central part of the study area. However, the fracturing was essentially undeveloped in the southwest of the study area.
(5) The reliability of the fracture prediction results was verified using fracture distribution statistics and gas production test results. Considering that the core area of the anticline in the PZ6-4 platform is the largest, and as the oblique fractures in these areas are developed, it is recommended to conduct more horizontal drilling in the PZ6-4 platform.

Author Contributions: Conceptualization, G.L.; supervision, G.L.; methodology, G.L. and Q.X.; software, Q.X.; data curation, H.P.; writing-original draft, Q.X.; writing-review and editing, X.Y. All authors have read and agreed to the published version of the manuscript.

Funding: This work is supported by the National Natural Science Foundation of China (No.51674217).

Informed Consent Statement: Not applicable.

Data Availability Statement: The data presented in this study are available on request from the corresponding author.

Conflicts of Interest: The authors declare no conflict of interest.

References

1. Guo, J.C.; Xiao, Y.; Zhu, H.Y. A New Method for Fracturing Wells Reservoir Evaluation in Fractured Gas Reservoir. *Math. Probl. Eng.* **2014**, *2014*, 814284. [CrossRef]
2. Wang, H.Y. Hydraulic fracture propagation in naturally fractured reservoirs: Complex fracture or fracture networks. *J. Nat. Gas Sci. Eng.* **2019**, *68*, 102911. [CrossRef]
3. Feng, J.W.; Qu, J.H.; Wan, H.Q.; Ren, Q.Q. Quantitative prediction of multiperiod fracture distributions in the Cambrian-Ordovician buried hill within the Futai Oilfield, Jiyang Depression, East China. *J. Struct. Geol.* **2021**, *148*, 104359. [CrossRef]
4. Ren, Q.Q.; Jin, Q.; Feng, J.W.; Li, Z.Y.; Du, H. Geomechanical models for the quantitatively prediction of multi-scale fracture distribution in carbonate reservoirs. *J. Struct. Geol.* **2020**, *135*, 104033. [CrossRef]
5. Wu, Y.S. *Multiphase Fluid Flow in Porous and Fractured Reservoirs*; Gulf Professional Publishing: Oxford, UK, 2015.
6. He, D.; Ma, Y.; Li, Y.; Wu, S. New directions in an established gas play: Promising dolomite reservoirs in the Middle Triassic Leikoupo Formation of the Sichuan Basin, China. *AAPG Bull.* **2019**, *103*, 1–29. [CrossRef]
7. Qin, S.; Zhang, B.; Huang, C.; Li, J.; Wang, J.; Tao, G.; Zhou, Z. Genetic Type and Source Analysis of Natural Gas in the Leikoupo Formation of the Sichuan Basin in China. *Front. Earth Sci.* **2022**, *10*, 891252. [CrossRef]
8. Wang, Y.; Jiang, W.; Liu, H.; Liu, B.; Zheng, H.; Song, X.; Wang, Q.; Wang, W.; Li, Y. Sedimentary and Diagenetic Features and Their Impacts on Microbial Carbonate Reservoirs in the Fourth Member of the Middle Triassic Leikoupo Formation, Western Sichuan Basin, China. *Energies* **2020**, *13*, 2293. [CrossRef]
9. Hu, X.; Zhao, X.; Su, Y.; Xiao, K.; Deng, M.; Wang, Q.; Liu, R. Formation mechanism of fractures in the carbonate reservoir of the 4th Member of Middle Triassic Leikoupo Fm in Longmenshan piedmont, Sichuan Basin. *Nat. Gas Ind.* **2018**, *38*, 15–25. (In Chinese)
10. Feng, Y.; Li, G.; Meng, Y.F.; Guo, B.Y. A Novel Approach to Investigating Transport of Lost Circulation Materials in Rough Fracture. *Energies* **2018**, *11*, 2572. [CrossRef]
11. Lai, J.; Wang, G.; Fan, Z.; Wang, Z.; Chen, J.; Zhou, Z.; Wang, S.; Xiao, C. Fracture detection in oil-based drilling mud using a combination of borehole image and sonic logs. *Mar. Pet. Geol.* **2017**, *84*, 195–214. [CrossRef]
12. Baytok, S.; Pranter, M.J. Fault and fracture distribution within a tight-gas sandstone reservoir: Mesaverde Group, Mamm Creek Field, Piceance Basin, Colorado, USA. *Pet. Geosci.* **2013**, *19*, 203–222. [CrossRef]
13. Bisdom, K.; Bertotti, G.; Nick, H.M. The impact of in-situ stress and outcrop-based fracture geometry on hydraulic aperture and upscaled permeability in fractured reservoirs. *Tectonophysics* **2016**, *690*, 63–75. [CrossRef]
14. Hardebol, N.J.; Bertotti, G. DigiFract: A software and data model implementation for flexible acquisition and processing of fracture data from outcrops. *Comput. Geosci.* **2013**, *54*, 326–336. [CrossRef]
15. Aghli, G.; Soleimani, B.; Moussavi-Harami, R.; Mohammadian, R. Fractured zones detection using conventional petrophysical logs by differentiation method and its correlation with image logs. *J. Petrol. Sci. Eng.* **2016**, *142*, 152–162. [CrossRef]
16. Griffith, W.A.; Prakash, V. Integrating field observations and fracture mechanics models to constrain seismic source parameters for ancient earthquakes. *Geology* **2015**, *43*, 763–766. [CrossRef]
17. Wilson, T.H.; Smith, V.; Brown, A. Developing a model discrete fracture network, drilling, and enhanced oil recovery strategy in an unconventional naturally fractured reservoir using integrated field, image log, and three-dimensional seismic data. *AAPG Bull.* **2015**, *99*, 735–762. [CrossRef]
18. Wu, Z.H.; Zuo, Y.J.; Wang, S.Y.; Yi, T.S.; Chen, S.J.; Yu, Q.L.; Li, W.; Sunwen, J.B.; Xu, Y.F.; Wang, R.Y.; et al. Numerical simulation and fractal analysis of mesoscopic scale failure in shale using digital images. *J. Petrol. Sci. Eng.* **2016**, *145*, 592–599. [CrossRef]
19. Guo, P.; Yao, L.H.; Ren, D.S. Simulation of three-dimensional tectonic stress fields and quantitative prediction of tectonic fracture within the Damintun Depression, Liaohe Basin, northeast China. *J. Struct. Geol.* **2016**, *86*, 211–223. [CrossRef]
20. Jiu, K.; Ding, W.L.; Huang, W.H.; You, S.G.; Zhang, Y.Q.; Zeng, W.T. Simulation of paleotectonic stress fields within Paleogene shale reservoirs and prediction of favorable zones for fracture development within the Zhanhua Depression, Bohai Bay Basin, east China. *J. Petrol. Sci. Eng.* **2013**, *110*, 119–131. [CrossRef]
21. Liu, J.S.; Ding, W.L.; Dai, J.S.; Gu, Y.; Yang, H.M.; Sun, B. Quantitative multiparameter prediction of fault-related fractures: A case study of the second member of the Funing Formation in the Jinhu Sag, Subei Basin. *Pet. Sci.* **2018**, *15*, 468–483. [CrossRef]
22. Ding, W.; Fan, T.; Yu, B.; Huang, X.; Liu, C. Ordovician carbonate reservoir fracture characteristics and fracture distribution forecasting in the Tazhong area of Tarim Basin, Northwest China. *J. Petrol. Sci. Eng.* **2012**, *86–87*, 62–70. [CrossRef]
23. Feng, J.W.; Ren, Q.Q.; Xu, K. Quantitative prediction of fracture distribution using geomechanical method within Kuqa Depression, Tarim Basin, NW China. *J. Petrol. Sci. Eng.* **2018**, *162*, 22–34. [CrossRef]
24. Ju, W.; Wang, J.L.; Fang, H.H.; Sun, W.F. Paleotectonic stress field modeling and prediction of natural fractures in the Lower Silurian Longmaxi shale reservoirs, Nanchuan region, South China. *Mar. Pet. Geol.* **2019**, *100*, 20–30. [CrossRef]
25. Smart, K.J.; Ferrill, D.A.; Morris, A.P.; McGinnis, R.N. Geomechanical modeling of stress and strain evolution during contractional fault-related folding. *Tectonophysics* **2012**, *576*, 171–196. [CrossRef]
26. Guo, P.; Ren, D.S.; Xue, Y.H. Simulation of multi-period tectonic stress fields and distribution prediction of tectonic fractures in tight gas reservoirs: A case study of the Tianhuan Depression in western Ordos Basin, China. *Mar. Pet. Geol.* **2019**, *109*, 530–546. [CrossRef]
27. Henk, A.; Nemcok, M. Stress and fracture prediction in inverted half-graben structures. *J. Struct. Geol.* **2008**, *30*, 81–97. [CrossRef]

28. Zeng, L.B.; Liu, H.T. Influence of fractures on the development of low-permeability sandstone reservoirs: A case study from the Taizhao district, Daqing Oilfield, China. *J. Petrol. Sci. Eng.* **2010**, *72*, 120–127. [CrossRef]
29. Zeng, L.B.; Wang, H.J.; Gong, L.; Liu, B.M. Impacts of the tectonic stress field on natural gas migration and accumulation: A case study of the Kuqa Depression in the Tarim Basin, China. *Mar. Pet. Geol.* **2010**, *27*, 1616–1627. [CrossRef]
30. Abdollahipour, A.; Marji, M.F. A thermo-hydromechanical displacement discontinuity method to model fractures in high-pressure, high-temperature environments. *Renewable Energy* **2020**, *153*, 1488–1503. [CrossRef]
31. Abdollahipour, A.; Marji, M.F.; Bafghi, A.Y.; Gholamnejad, J. Time-dependent crack propagation in a poroelastic medium using a fully coupled hydromechanical displacement discontinuity method. *Int. J. Fract.* **2016**, *199*, 71–87. [CrossRef]
32. Haeri, H.; Sarfarazi, V.; Ebneabbasi, P.; Maram, A.N.; Shahbazian, A.; Marji, M.F.; Mohamadi, A.R. XFEM and experimental simulation of failure mechanism of non-persistent joints in mortar under compression. *Constr. Build. Mater.* **2020**, *236*, 117500. [CrossRef]
33. Liu, Y.; Ding, Z.; Qu, Y.; Zhao, C. The characterization of fracture orientation and the calculation of anisotropic permeability parameters of reservoirs. *Acta Pet. Sin.* **2011**, *32*, 842–846.
34. Hu, X.; Deng, H.; He, J.; Shen, Z.; Peng, X. Complex genesis of multiperiod fractures in the Middle Triassic Leikoupo Formation in the Pengzhou gas field, western Sichuan Basin, China. *Pet. Sci.* **2022**. [CrossRef]
35. Song, X.B.; Liu, S.R.; Wang, Q.X.; Deng, D.P. Main controlling factors of hydrocarbon accumulation of Middle-Lower Triassic in western margin of western Sichuan Depression. *Lithol. Reserv.* **2011**, *23*, 67–73. (In Chinese)
36. Fjær, E.; Holt, R.; Horsrud, P.; Risnes, R. *Petroleum Related Rock Mechanics*, 2nd ed.; Elsevier: Amsterdam, The Netherlands, 2008.
37. Liu, J.; Ding, W.; Wang, R.; Yang, H.; Wang, X.; Li, A. Methodology for quantitative prediction of fracture sealing with a case study of the lower Cambrian Niutitang Formation in the Cen'gong block in South China. *J. Petrol. Sci. Eng.* **2018**, *160*, 565–581. [CrossRef]
38. Yin, S.; Wu, Z. Geomechanical simulation of low-order fracture of tight sandstone. *Mar. Pet. Geol.* **2020**, *117*, 104359. [CrossRef]
39. Zoback, M.D. *Reservoir Geomechanics*; Cambridge University Press: London, UK, 2007.
40. Liu, J.; Ding, W.; Gu, Y.; Xiao, Z.; Dai, J.; Dai, P.; Chen, X.; Zhao, G. Methodology for predicting reservoir breakdown pressure and fracture opening pressure in low-permeability reservoirs based on an in situ stress simulation. *Eng. Geol.* **2018**, *246*, 222–232. [CrossRef]
41. Zeng, W.T.; Ding, W.L.; Zhang, J.C.; Zhang, Y.Q.; Guo, L.; Jiu, K.; Li, Y.F. Fracture development in Paleozoic shale of Chongqing area (South China). Part two: Numerical simulation of tectonic stress field and prediction of fractures distribution. *J. Asian Earth Sci.* **2013**, *75*, 267–279. [CrossRef]
42. Ridd, M.F.; Watkinson, I. The Phuket-Slate Belt terrane: Tectonic evolution and strike-slip emplacement of a major terrane on the Sundaland margin of Thailand and Myanmar. *P. Geol. Assoc.* **2013**, *124*, 994–1010. [CrossRef]